East Asian Monsoon and its Interannual Variability

KOICA Expert Program

for

Climate Prediction in Asia-Pacific

2007

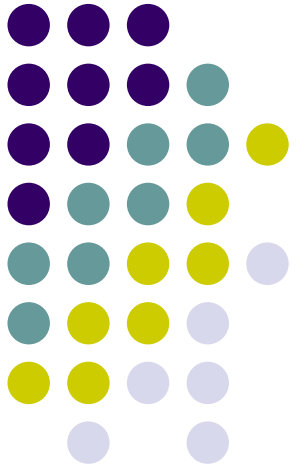

Overview of Monsoon

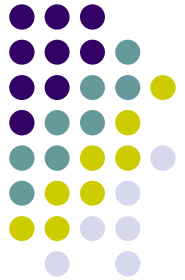

- Characteristics of monsoon circulation
- Evolution of East-Asian monsoon
- Monsoon breaks & Intraseasonal oscillation
- Synoptic-scale/TC activity

Characteristics of monsoon circulation and its evolution

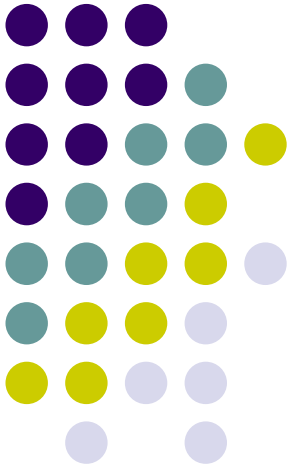

Precipitation and 1000mb wind- JJA & DJF

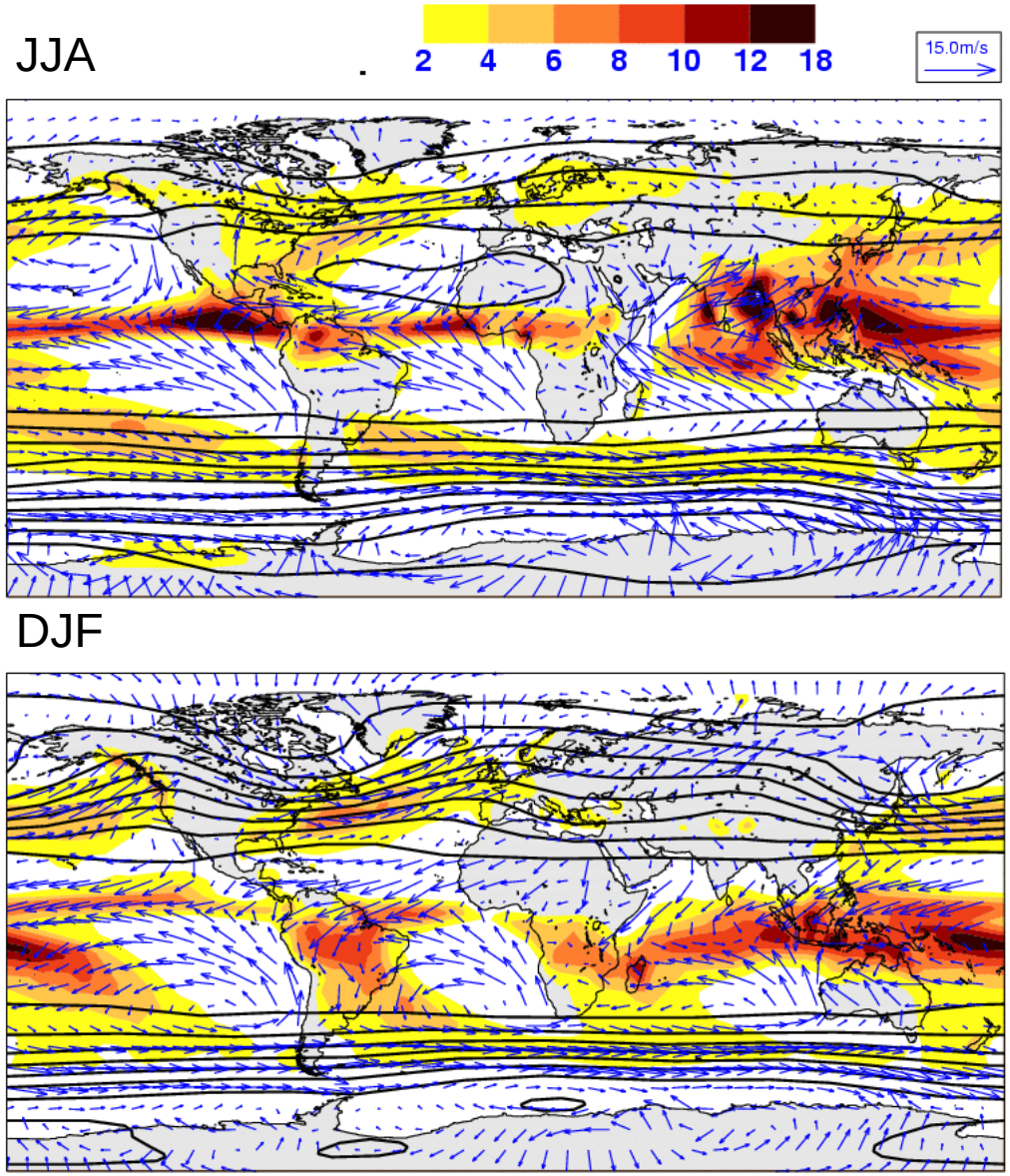

Precip. & 925mb wind: July-August minus January-February climatology

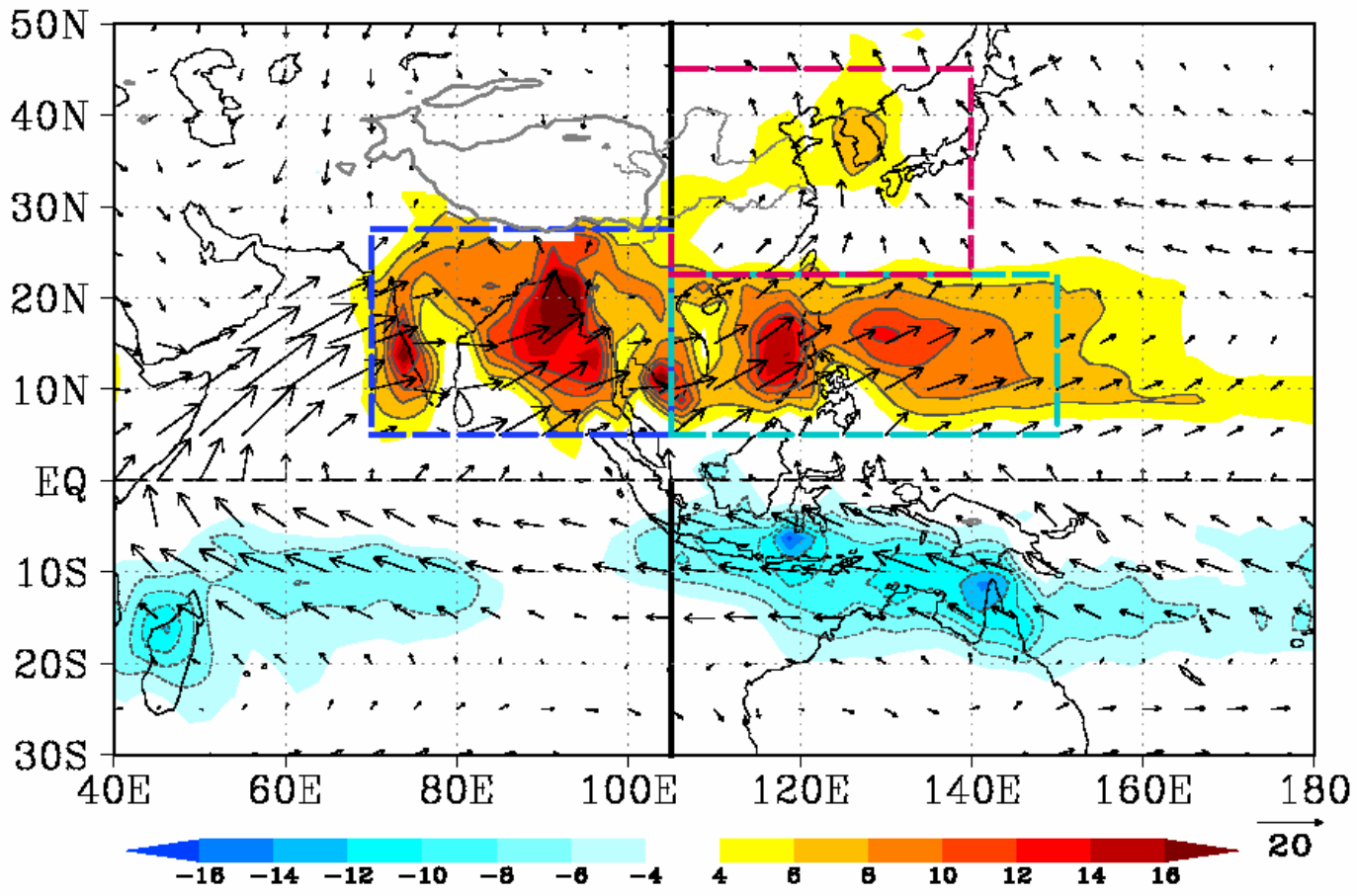

Seasonal march of subsystems

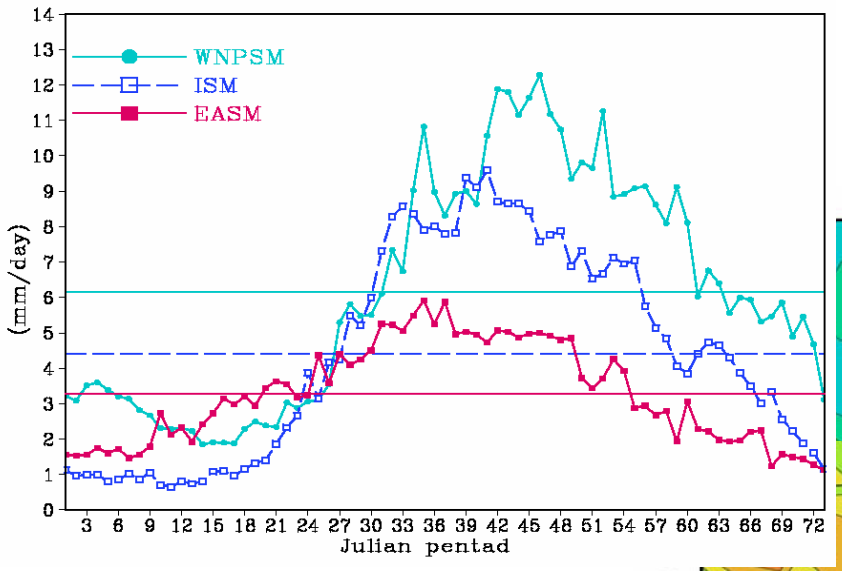

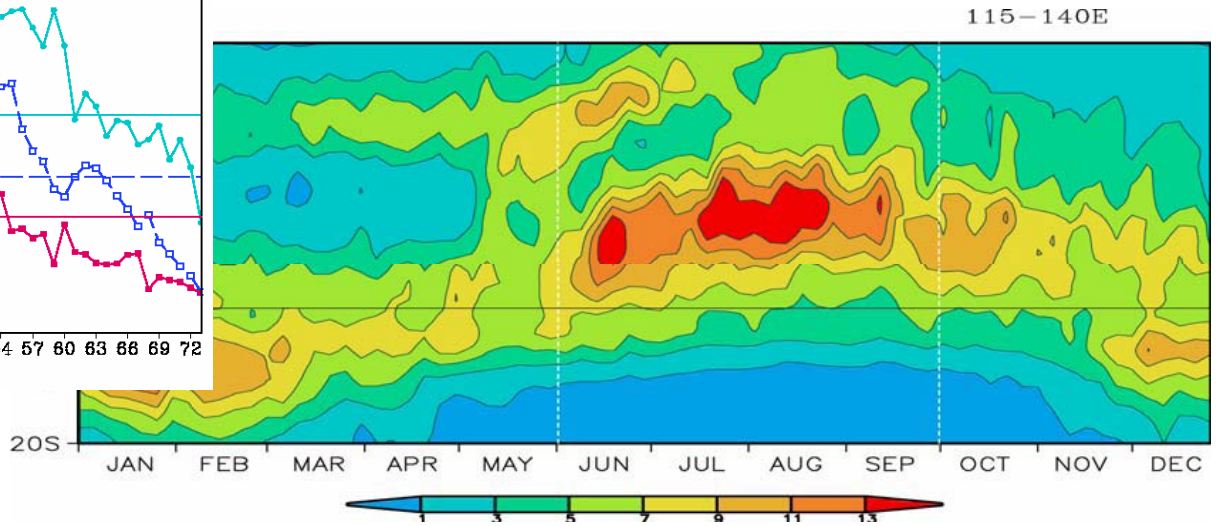

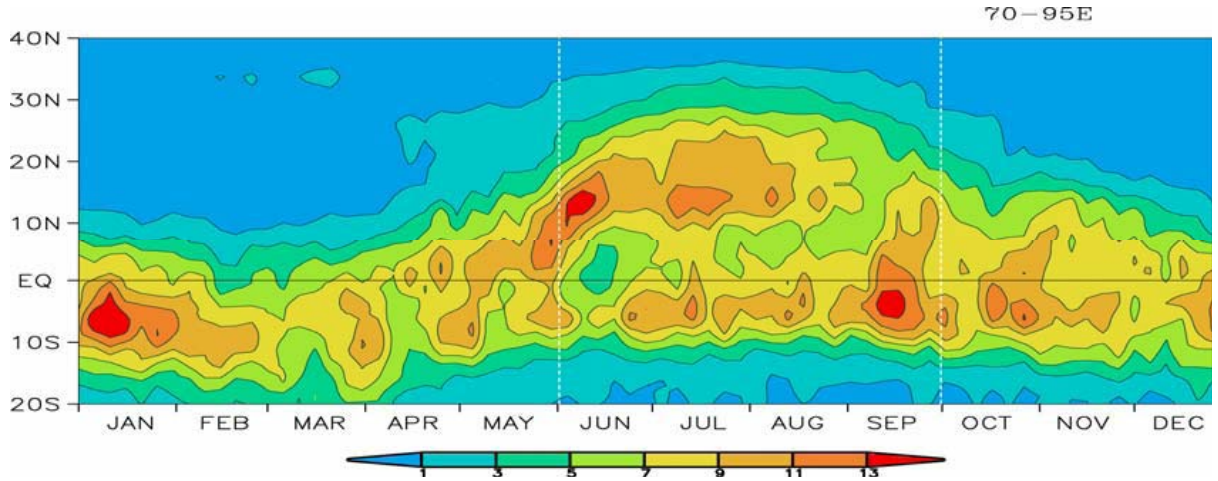

Northern summer monsoon onset

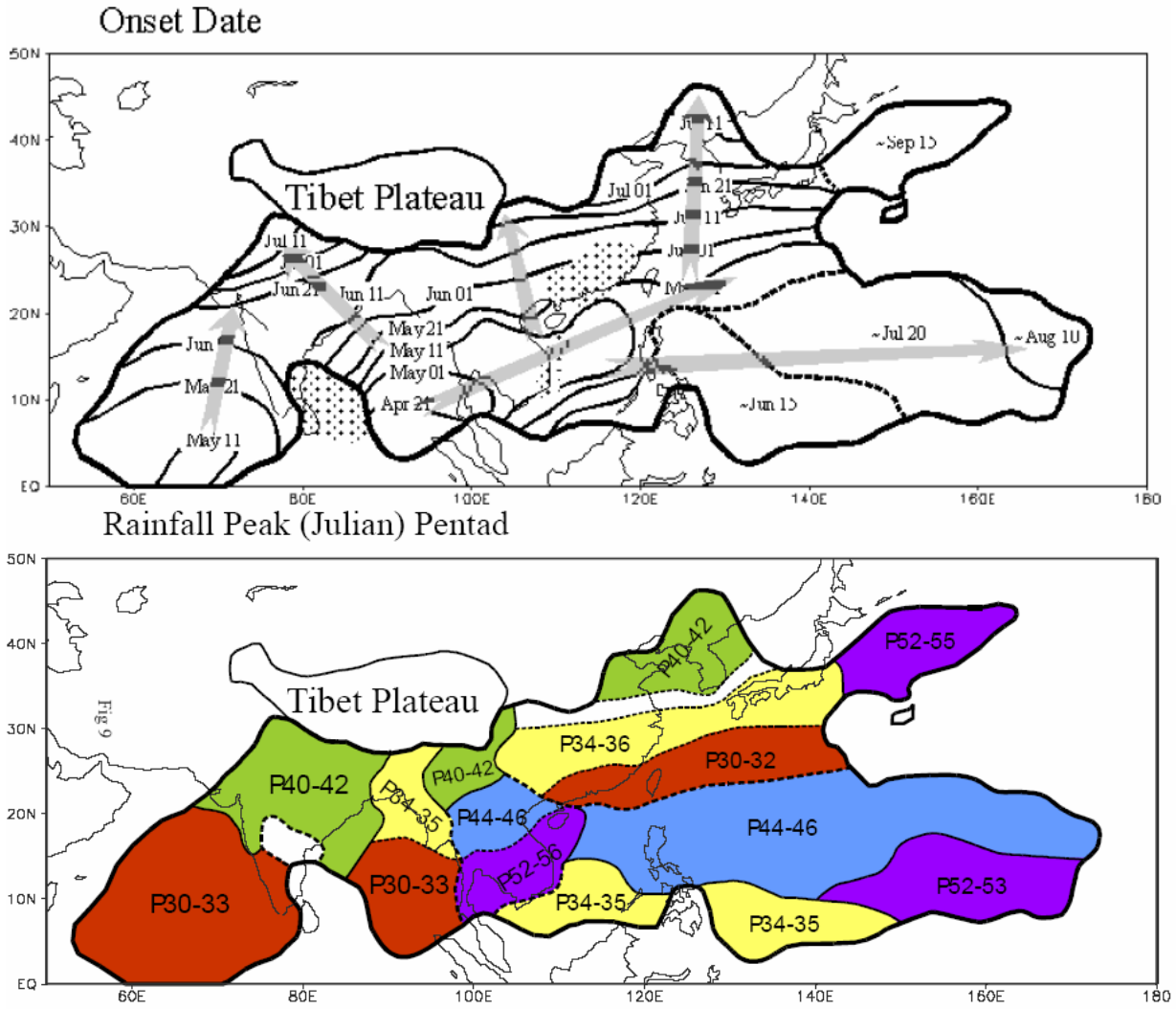

Asian summer monsoon rainy season characteristics: (a) onset and (b) peak pentad (Adapted from Wang and Lin 2002).

Monsoon breaks & Intraseasonal oscillation

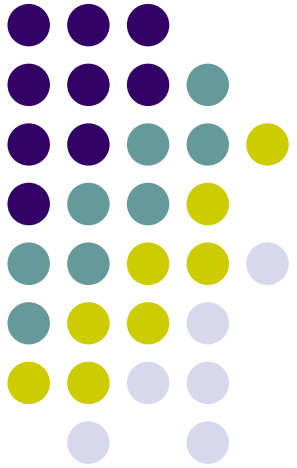

Monsoon break

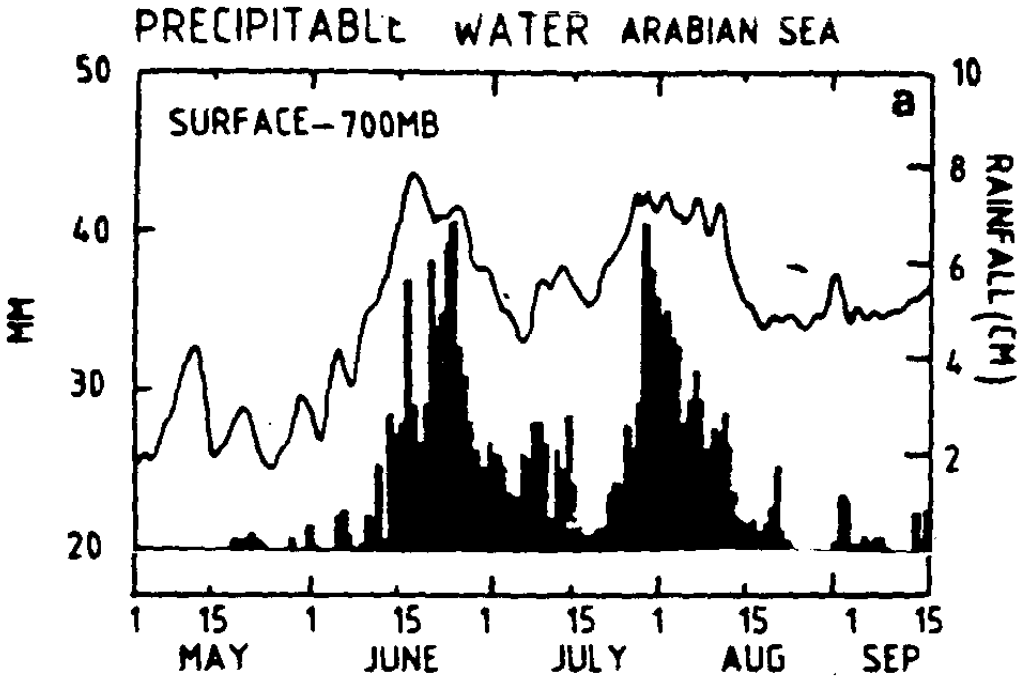

FIG. 10. Time series of the precipitable water from the surface to 700 hPa over the Arabian Sea (thin line) from *TIROS-N,* and the precipitation along the west coast of India during MONEX (adapted from Cadet 1986).

Monsoon break

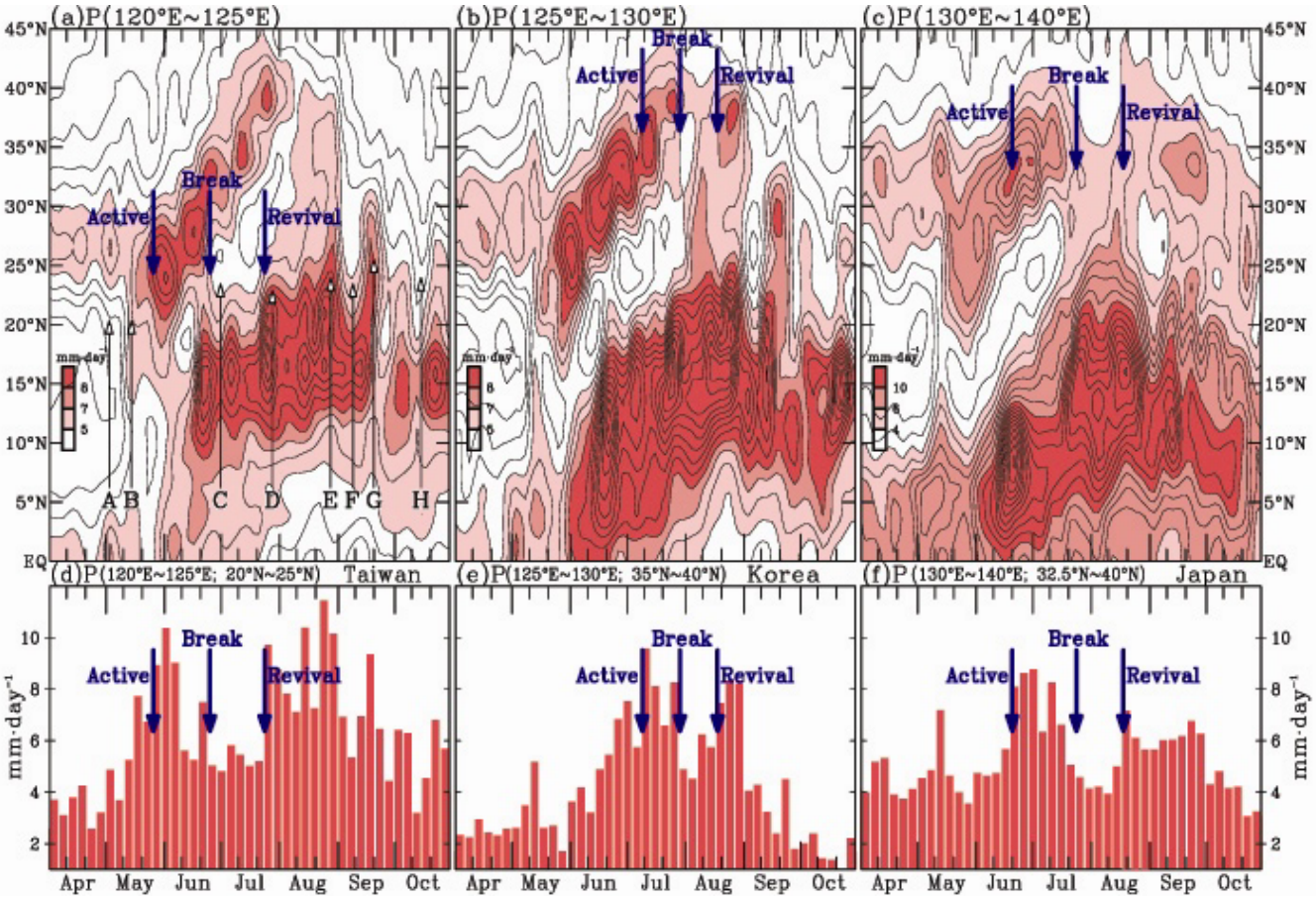

Latitudinal-time cross-sections of CMAP rainfall averaged over longitudinal zones of (a) 120°-125°E, (b) 125°-130°E, and (c) 130°-140°E, and rainfall histograms of three regions: (d) Taiwan (120°-125°E, 20-25°N), (e) Korea (125°-130°E, 35°-40°N), and (f) Japan (130°-140°E, 32.5°-40°N). Different phases of summer monsoons in three regions are indicated by active, break and revival. The contour interval of CMAP rainfall in (a)-(c) is 1 mm day-1, while rainfall amounts larger than 5 mm day^{-1} are stippled by different colors indicated by the scale shown in the lower left corner of the three upper panels. (Chen *et al.*, 2003)

Madden-Julian Oscillation (MJO)

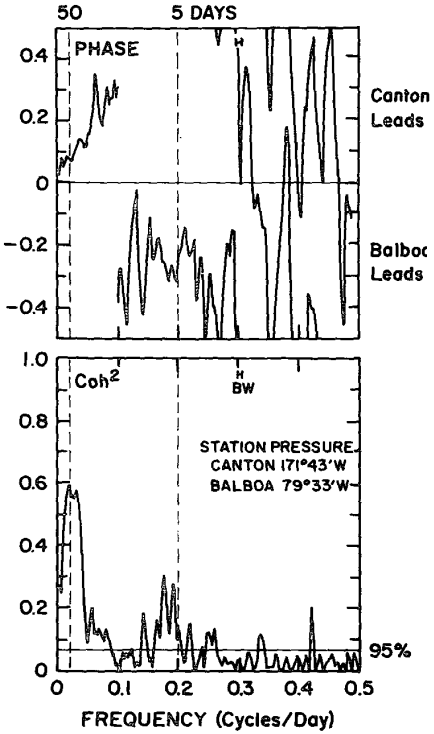

FIG. 1. Coherence squared (bottom) and phase in fractions of a cycle between the surface pressures at Canton (2.8°S, 171.7°W) and Balboa (9.0°N, 79.6°W) for the period 16 December 1959–24 March 1967. The bandwidth and the 95% limit for a null hypothesis of zero coherence are indicated.

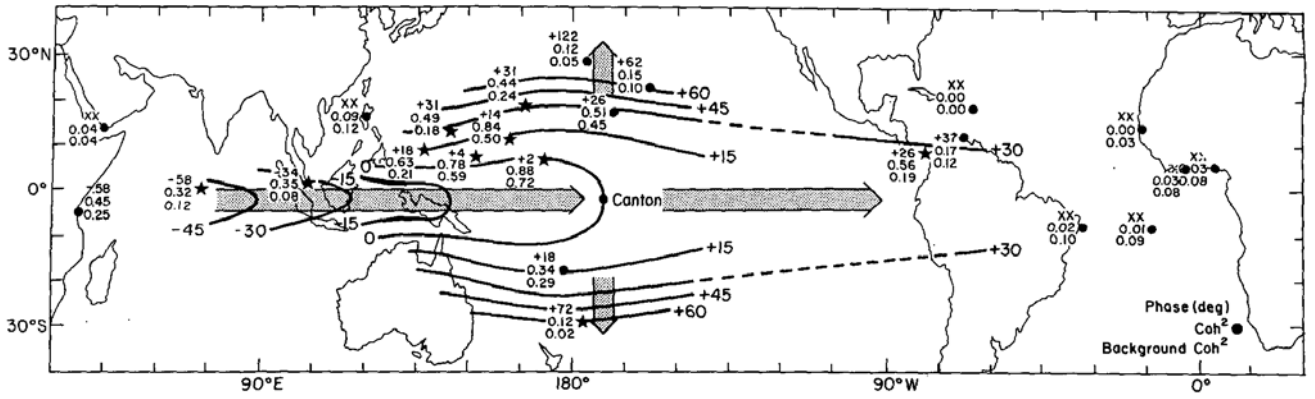

FIG. 2. Mean phase angles (deg), coherence squares, and background coherence squares for approximately the 36–50-day period range of cross spectra between surface pressures at all stations and those at Canton. The plotting model is given in the lower right-hand corner. Positive phase angle means Canton time series leads. Stars indicate stations where coherence squares exceed a smooth background at the 95% level. Mean coherence squares at Shemya (52.8°N, 174.1°E) and Campbell Island (52.6°S, 169.2°E) (not shown) are 0.08 and 0.02, respectively. Both are below their average background coherence squares. Values at Dar es Salaam (0.8°S, 39.3°E) are from a cross spectrum with Nauru. The arrows indicate propagation direction (adapted from Madden and Julian 1972).

Madden-Julian Oscillation (MJO)

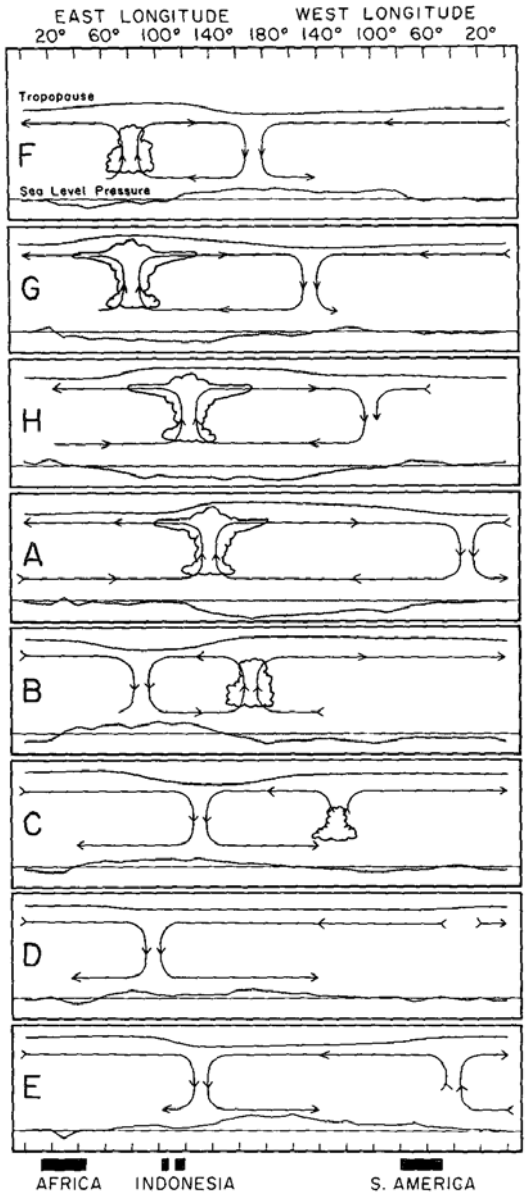

FIG. 3. Schematic depiction of the time and space (zonal plane) variations of the disturbance associated with the 40–50-day oscillation. Dates are indicated symbolically by the letters at the left of each chart and correspond to dates associated with the oscillation in Canton's station pressure. The letter A refers to the time of low pressure at Canton and E is the time of high pressure there. The other letters represent intermediate times. The mean pressure disturbance is plotted at the bottom of each chart with negative anomalies shaded. The circulation cells are based on the mean zonal wind disturbance. Regions of enhanced large-scale convection are indicated schematically by the cumulus and cumulonimbus clouds. The relative tropopause height is indicated at the top of each chart (taken from Madden and Julian 1972a).

Northward propagating intraseasonal activity in boreal summer

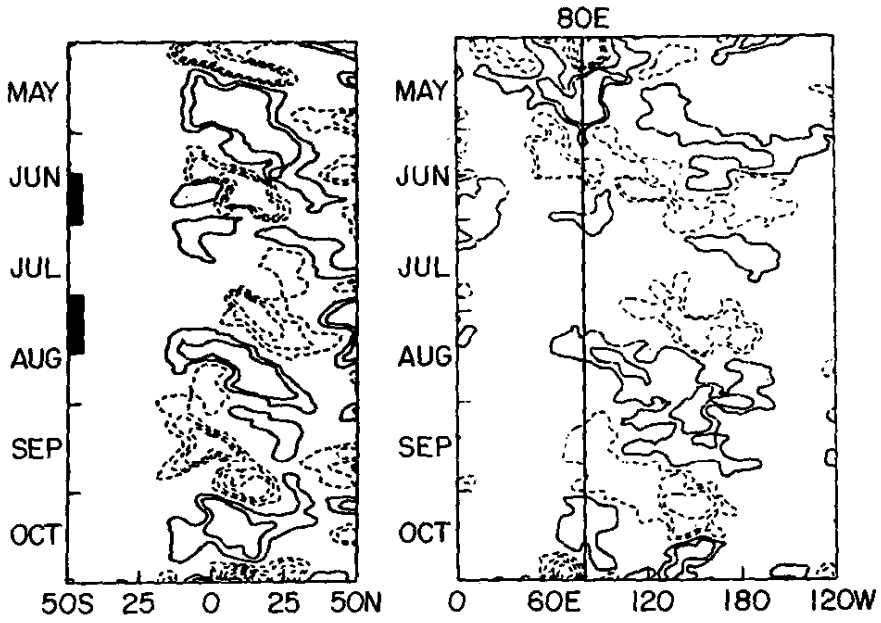

FIG. 11. Longitude–time section of anomalies in outgoing longwave radiation along the equator (5°S–5°N) during MONEX (right-hand side). Latitude–time section along 80°E (75°–85°E) for the same period (left-hand side). Contours are watts per square meter with negative values dashed and the zero contour suppressed. Times of active monsoon phases from Fig. 10 are indicated on the left-hand side by the dark bars (adapted from Lau and Chan 1986a).

Intraseasonal Oscillation- Boreal summer ISO

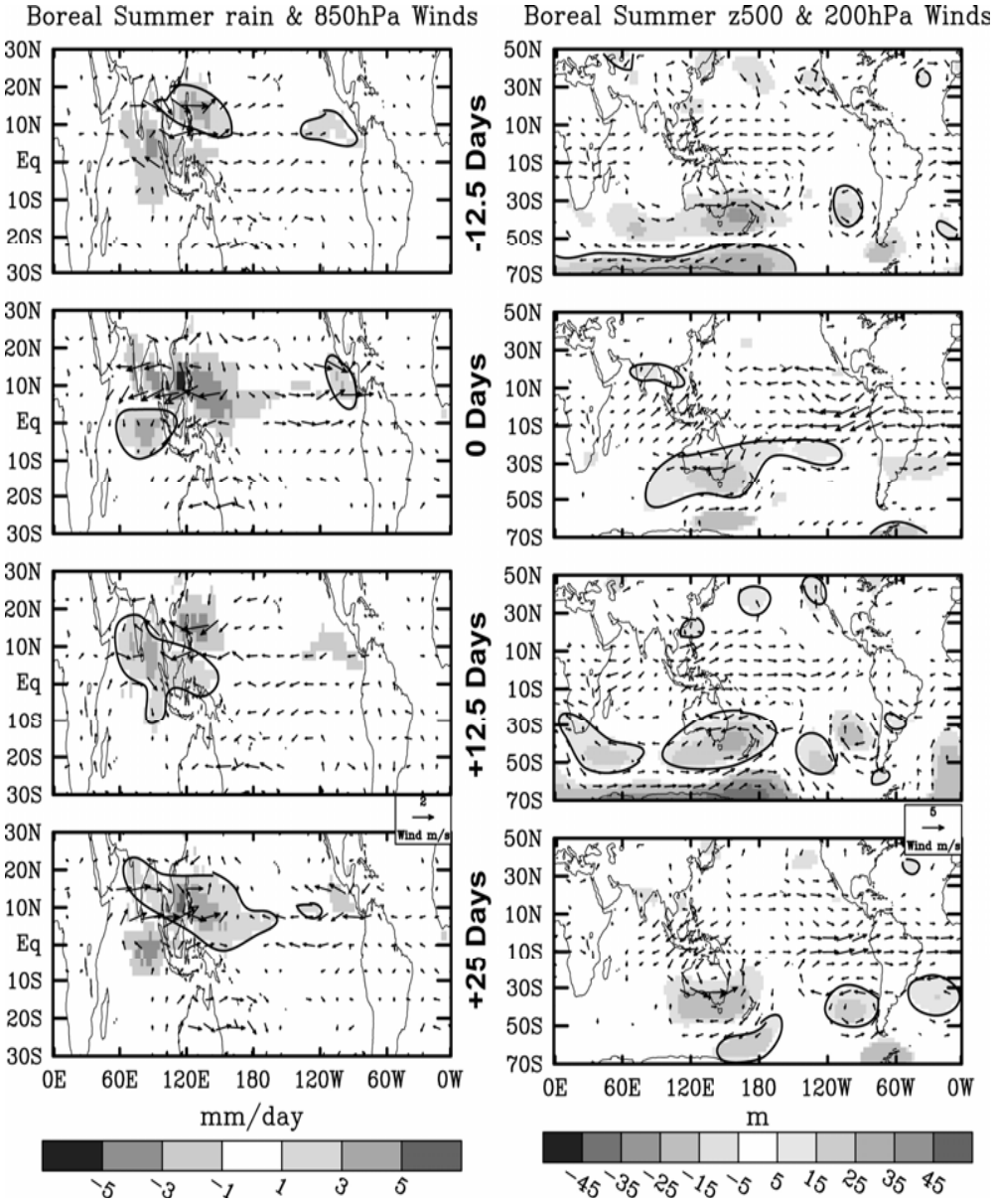

Canonical boreal summer ISO for May to October

Intraseasonal Oscillation-Boreal summer ISO

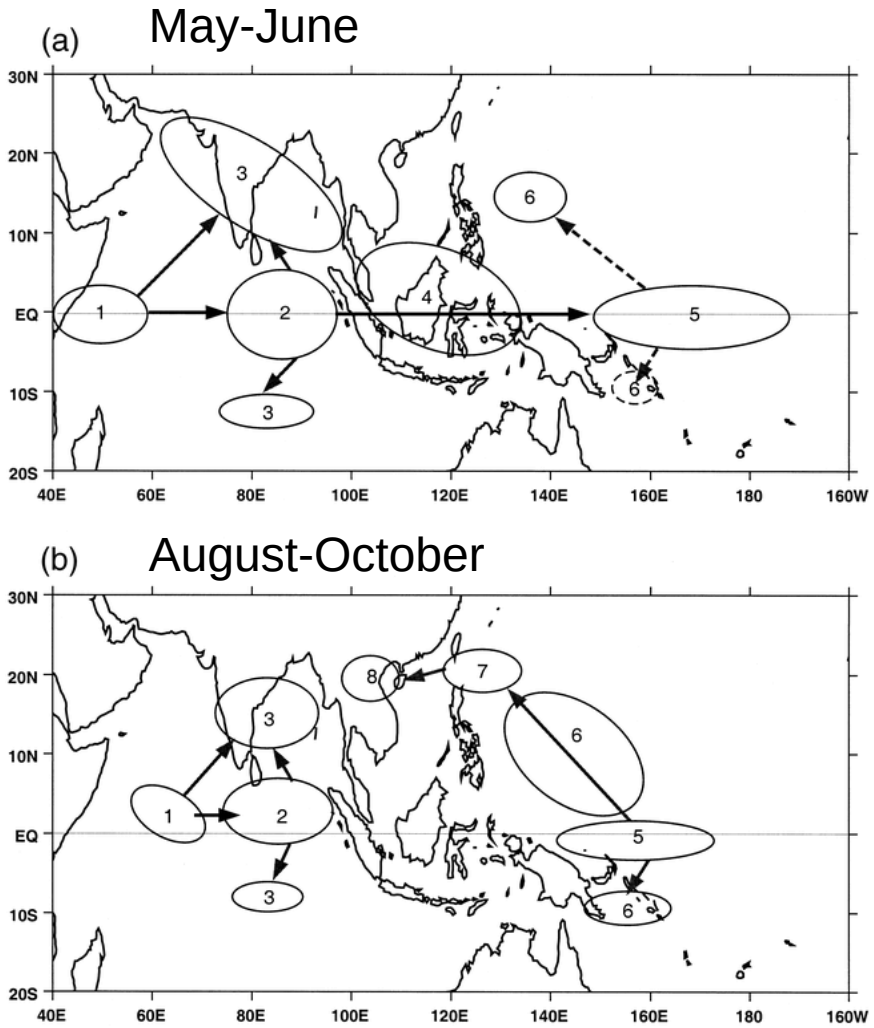

The schematic life cycle for intraseasonal convective anomalies constructed for (a) May–Jun and (b) Aug–Oct using OLR data (1979-1998). Ovals indicate convection, with numbers indicating the evolution of the anomaly. (Kemball-Cook and Wang 2001.)

(APCC's ISV monitoring product: http://210.98.49.34:3000/services/monitoring/analysis/isv/)

Intraseasonal Oscillation- effect on TC activity

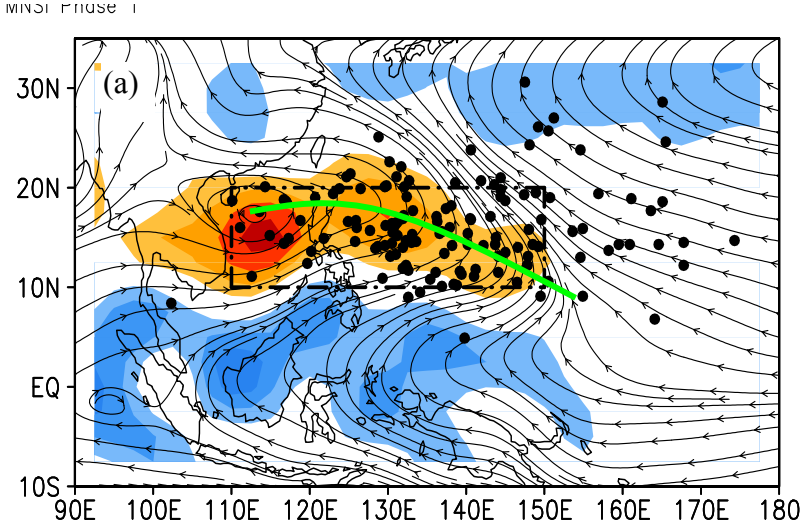

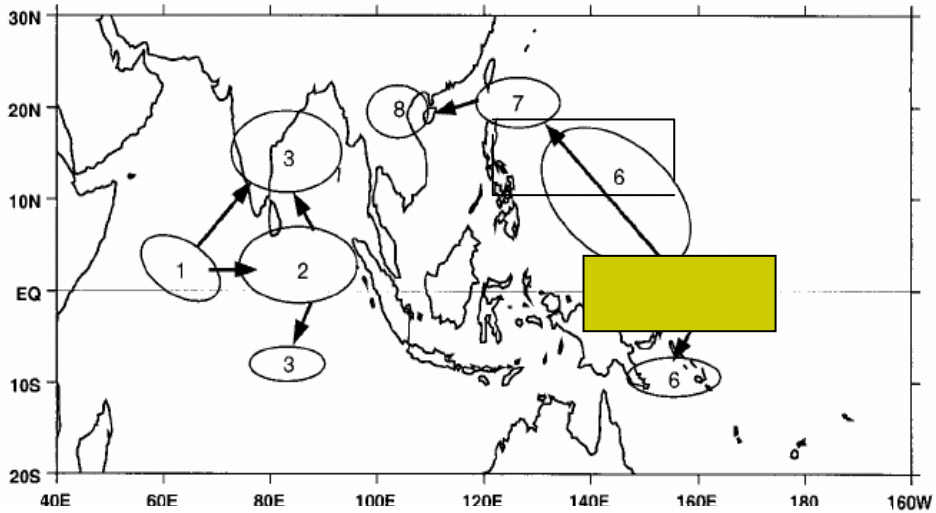

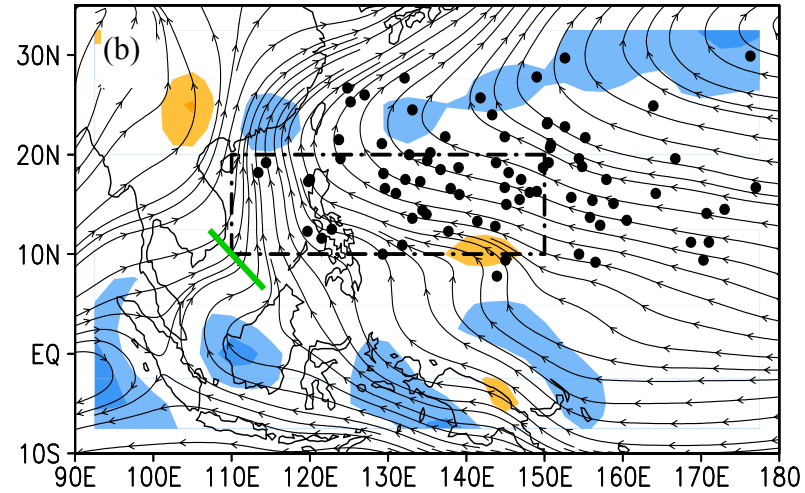

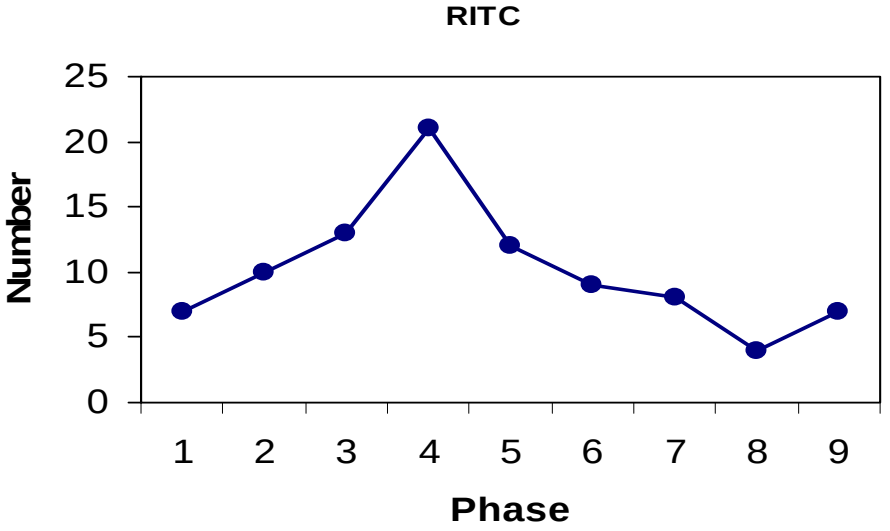

Frequency of rapidly intensifying TC during different phases of ISO (B. Wang, personnel communication)

Intraseasonal Oscillation- effect on TC activity

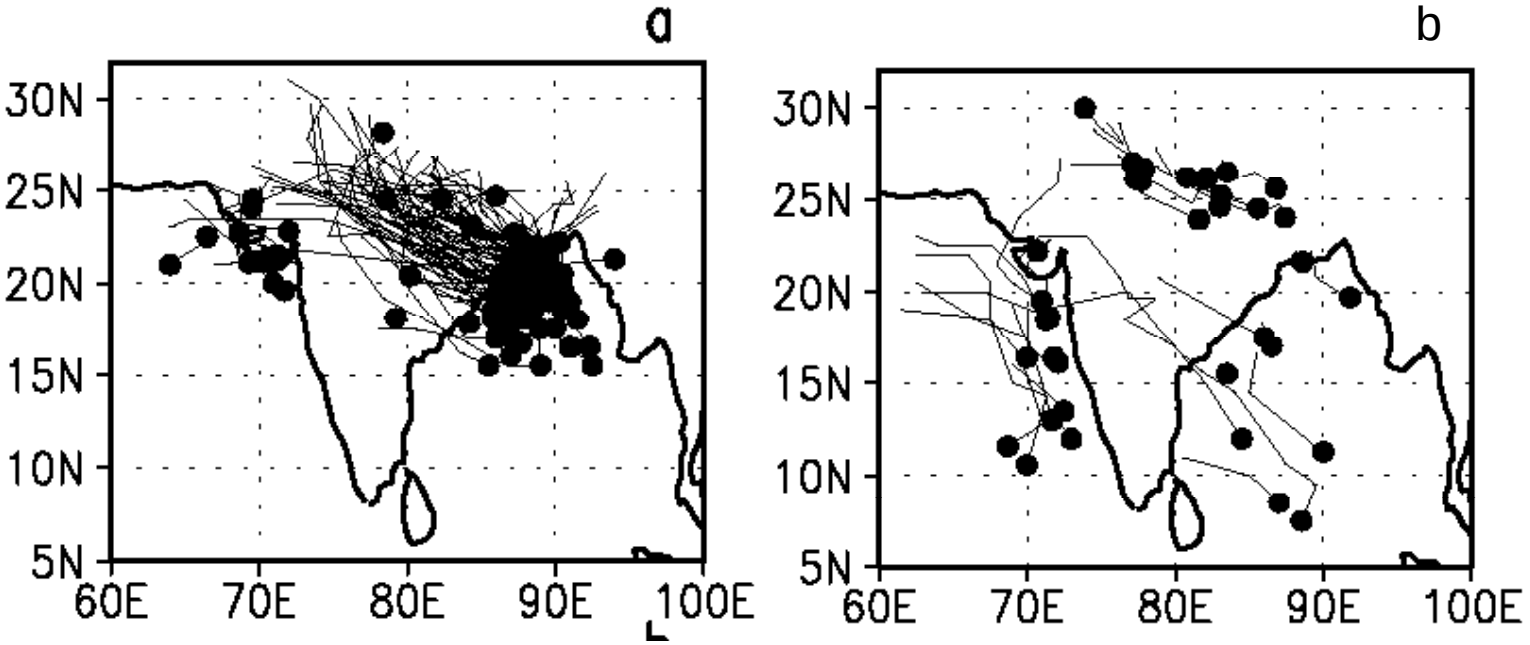

Tracks of low-pressure systems (LPS) for the period 1954–1983 during extreme phases of boreal summer ISO. (a) 'Active' ISO phase (analogous to 4th panel of Figure 4) and (b) 'Break' ISO phase (analogous to 2nd panel of Figure 4). Dark dots represent the genesis point of the LPS and their lines show the tracks. From Goswami et al. (2003).

Synoptic-scale/TC activity

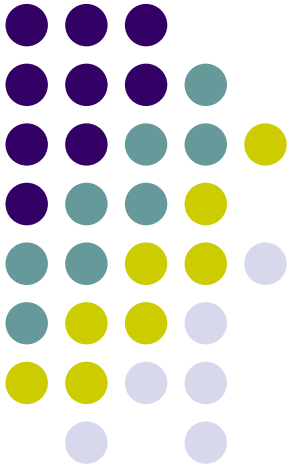

Summertime tropical synoptic-scale activity (easterly waves)

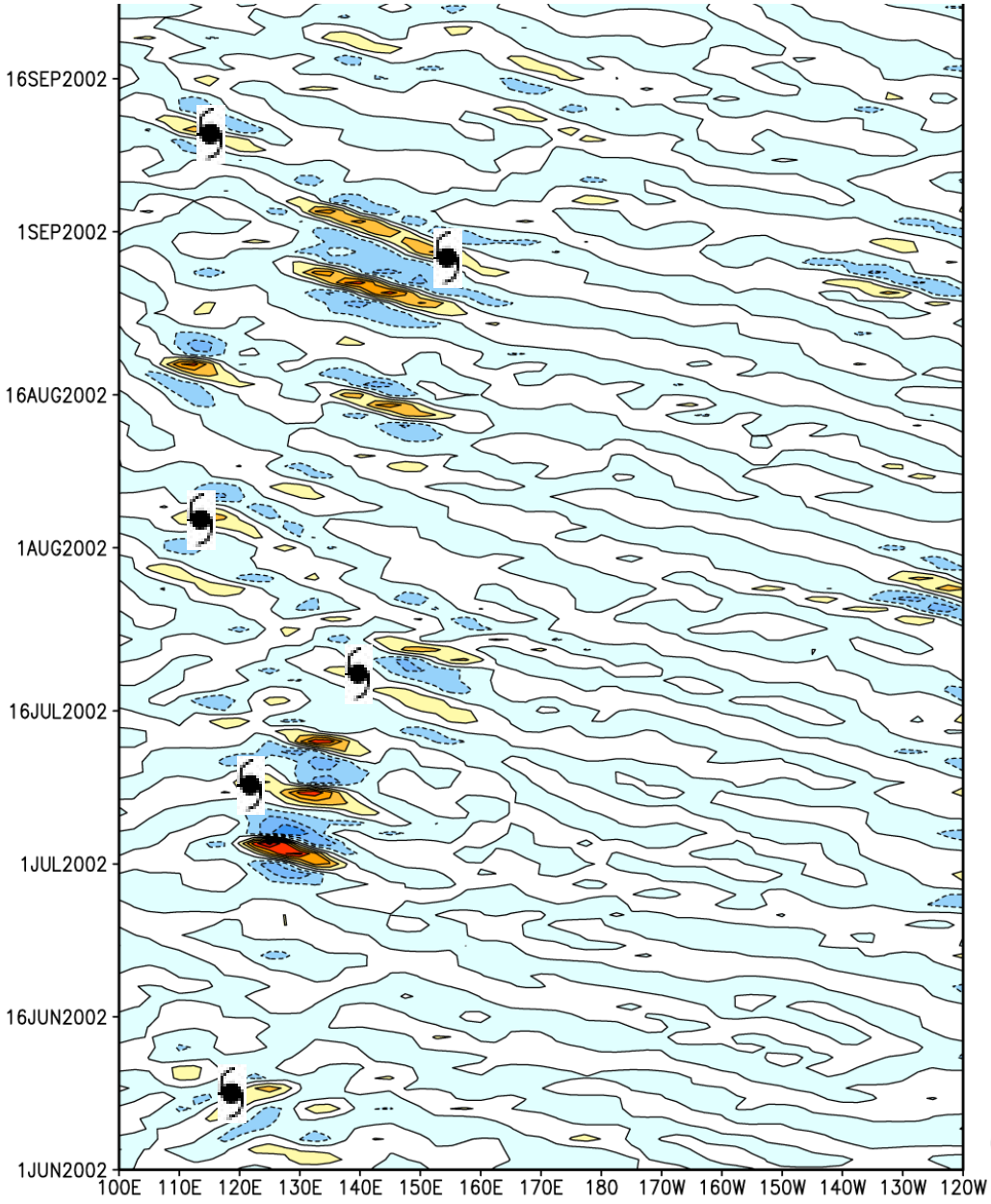

- Westward propagating
- 2000-4000km, period ~ 3-8dy
- Organized in wave packets
- Associated with TC activity

(850mb vorticity at 20N)

rms of 850mb vorticity for JJA

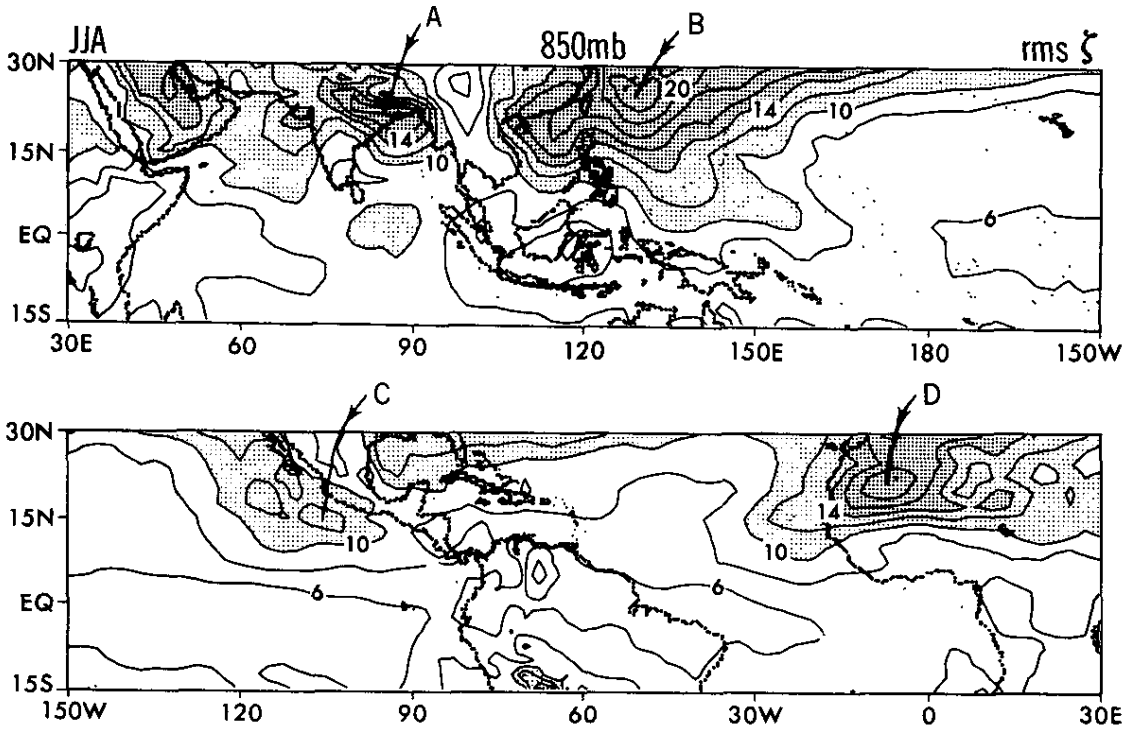

FIG. 1. Distribution of root-mean-squares of unfiltered vorticity fluctuations at 850 mb during the northern summer. Contour interval is 2×10^{-6} s^{-1}. Light stippling indicates values between 10×10^{-6} s^{-1} and 14×10^{-6} s^{-1}. Dense stippling indicates values greater than 14×10^{-6} s^{-1}.

(From Lau and Lau 90)

Spectra of 850mb vorticity

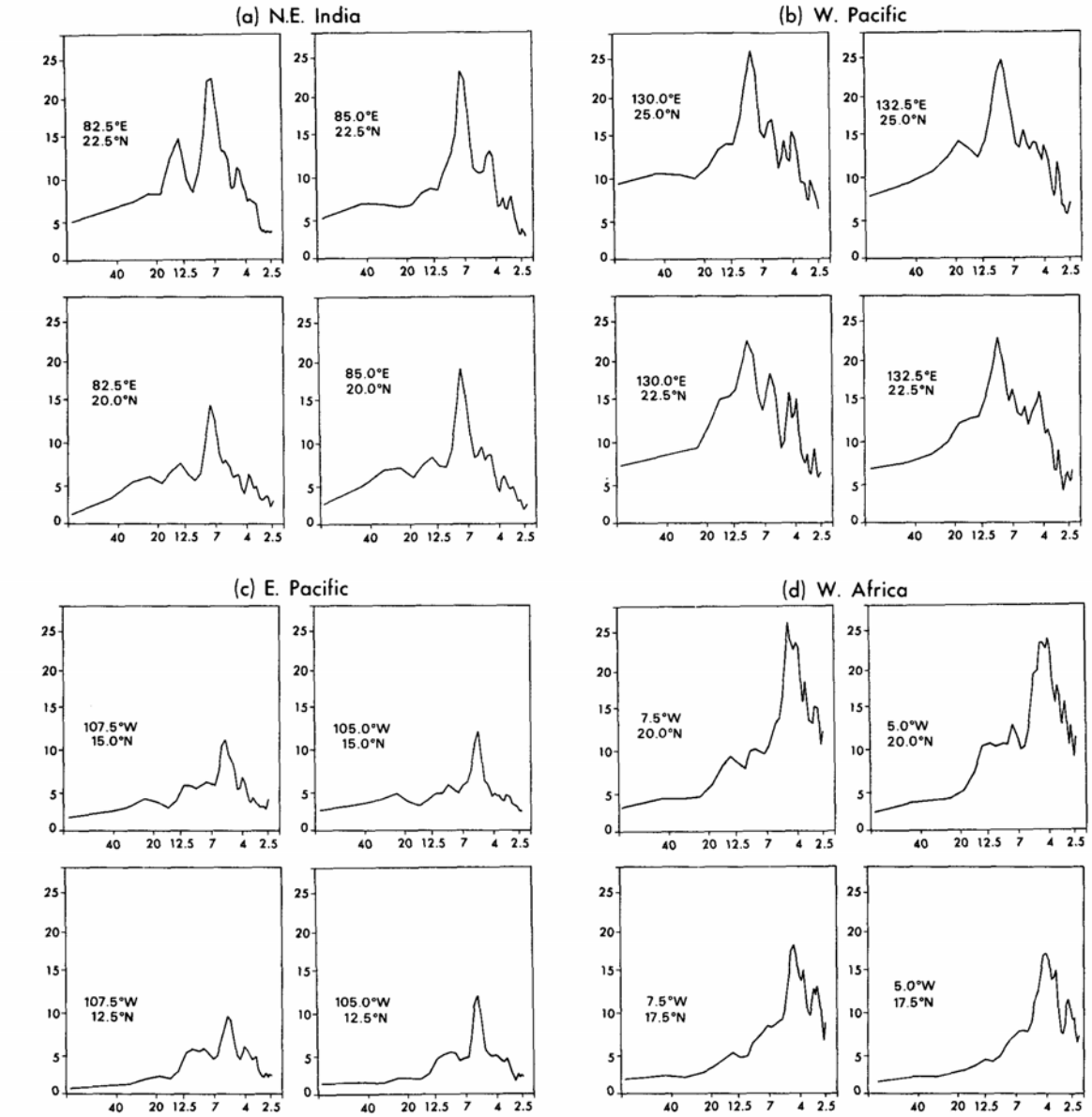

FIG. 3. Sample power spectra of relative vorticity, with $vP(v)$ plotted against $\ln(v)$, where v is the frequency and P is the power. The sites chosen correspond to maxima in the distribution of rms of vorticity in Fig. 1, and are marked as A, B, C, and D in that figure. These locations include (a) northeastern India, near 20°N, 85°E; (b) western Pacific, near 25°N, 130°E; (c) eastern Pacific, near 15°N, 105°W; and (d) western Africa, near 20°N, 5°W. Units are in day for the abscissa, and in 10^{-11} s^{-2} day^{-1} for the ordinate.

(From Lau and Lau 90)

1-pt lag correlation maps

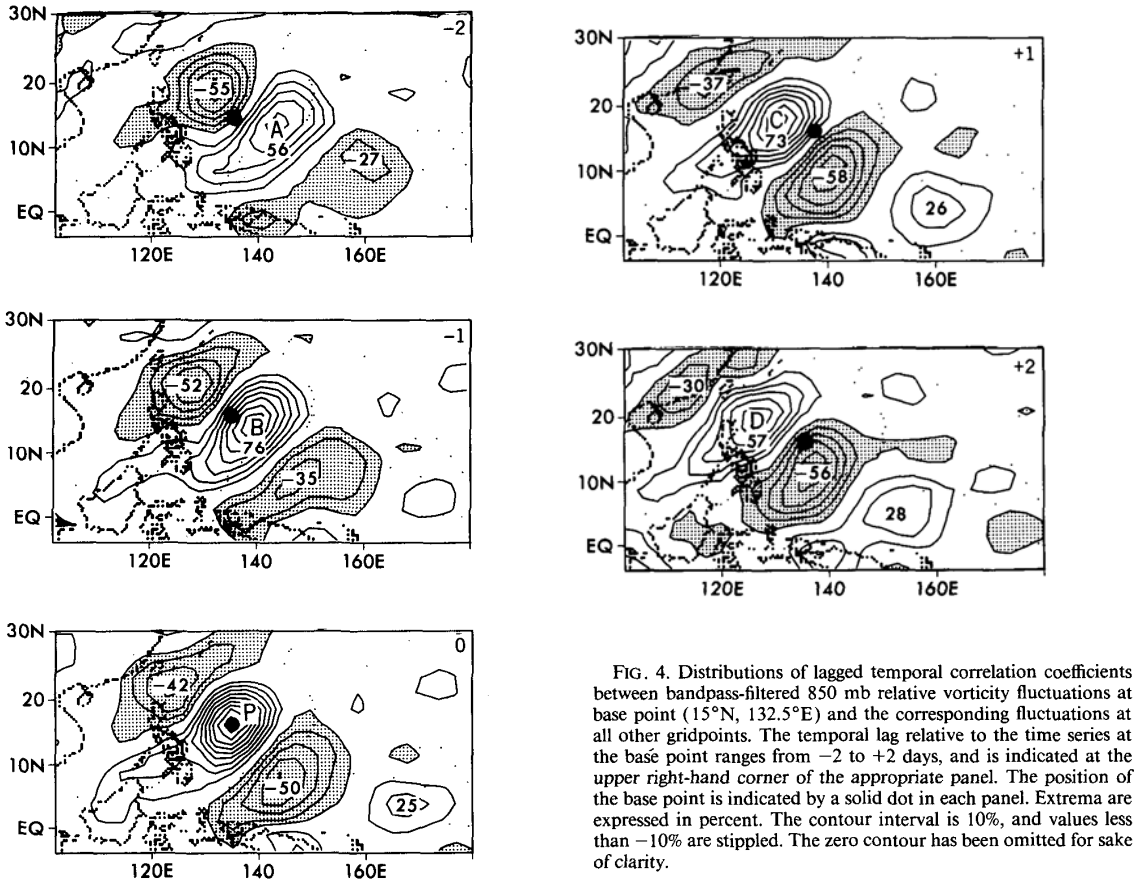

FIG. 4. Distributions of lagged temporal correlation coefficients between bandpass-filtered 850 mb relative vorticity fluctuations at base point (15°N, 132.5°E) and the corresponding fluctuations at all other gridpoints. The temporal lag relative to the time series at the base point ranges from −2 to +2 days, and is indicated at the upper right-hand corner of the appropriate panel. The position of the base point is indicated by a solid dot in each panel. Extrema are expressed in percent. The contour interval is 10%, and values less than −10% are stippled. The zero contour has been omitted for sake of clarity.

(From Lau and Lau 90)

Phase propagation vectors

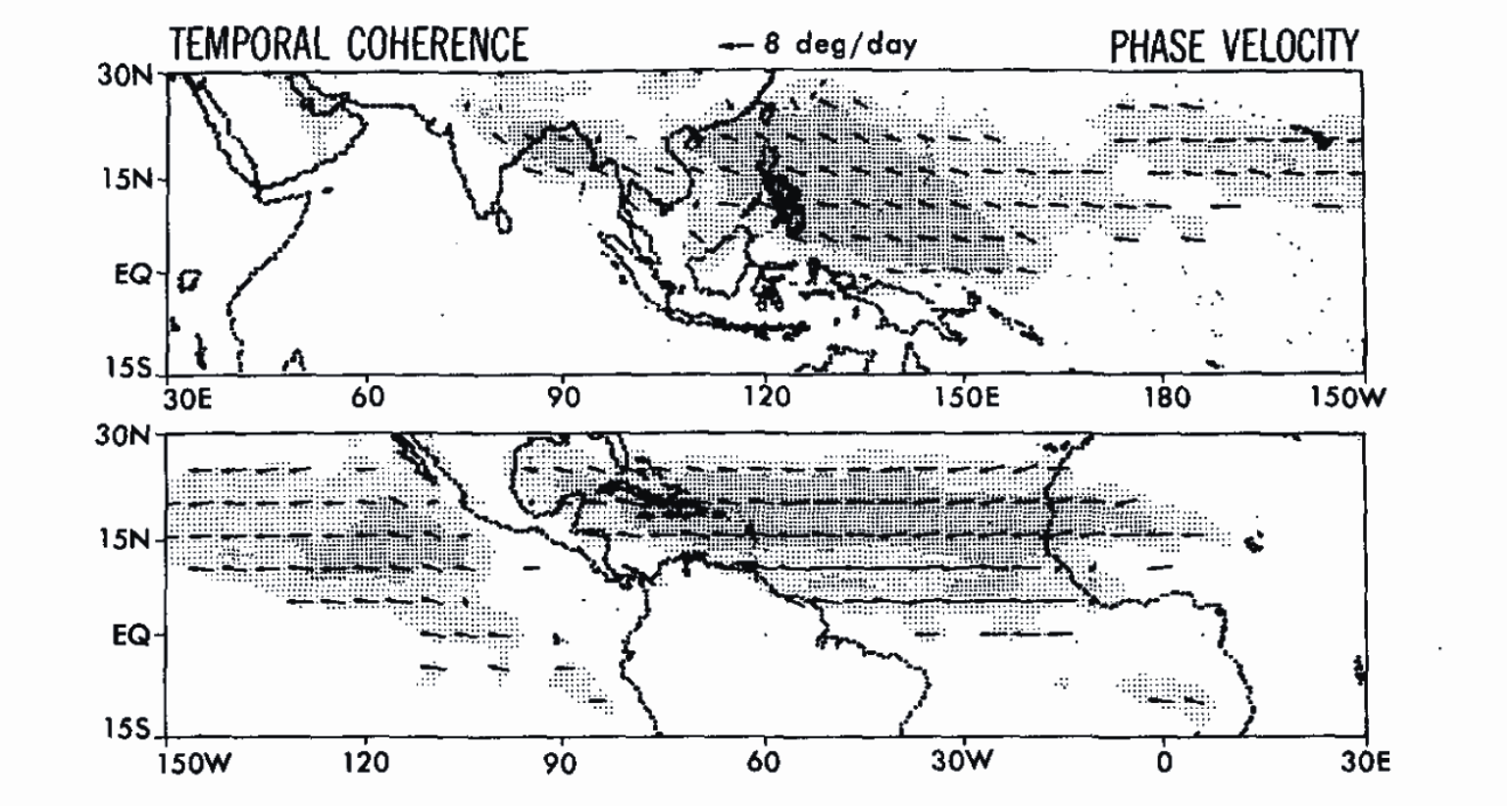

(Lau and Lau 90)

- Coherent, wave-like disturbances
- Westward/northwestward propagating

Growth/decay of synoptic-scale waves

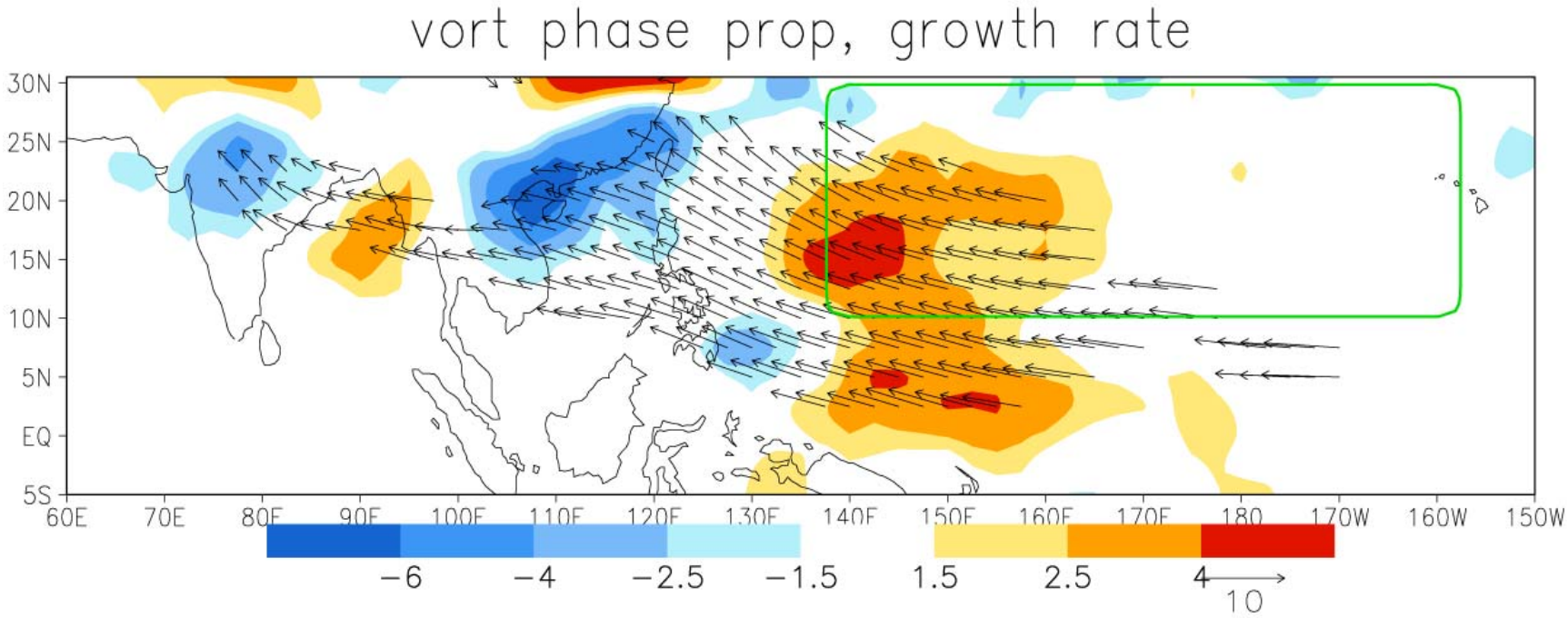

(based on 8-day hp filtered 850mb vorticitiy; see Lau and Lau 90)

Q: origin of disturbances over WPAC north of ~ 15N?

(based on Tam and Li 2006)

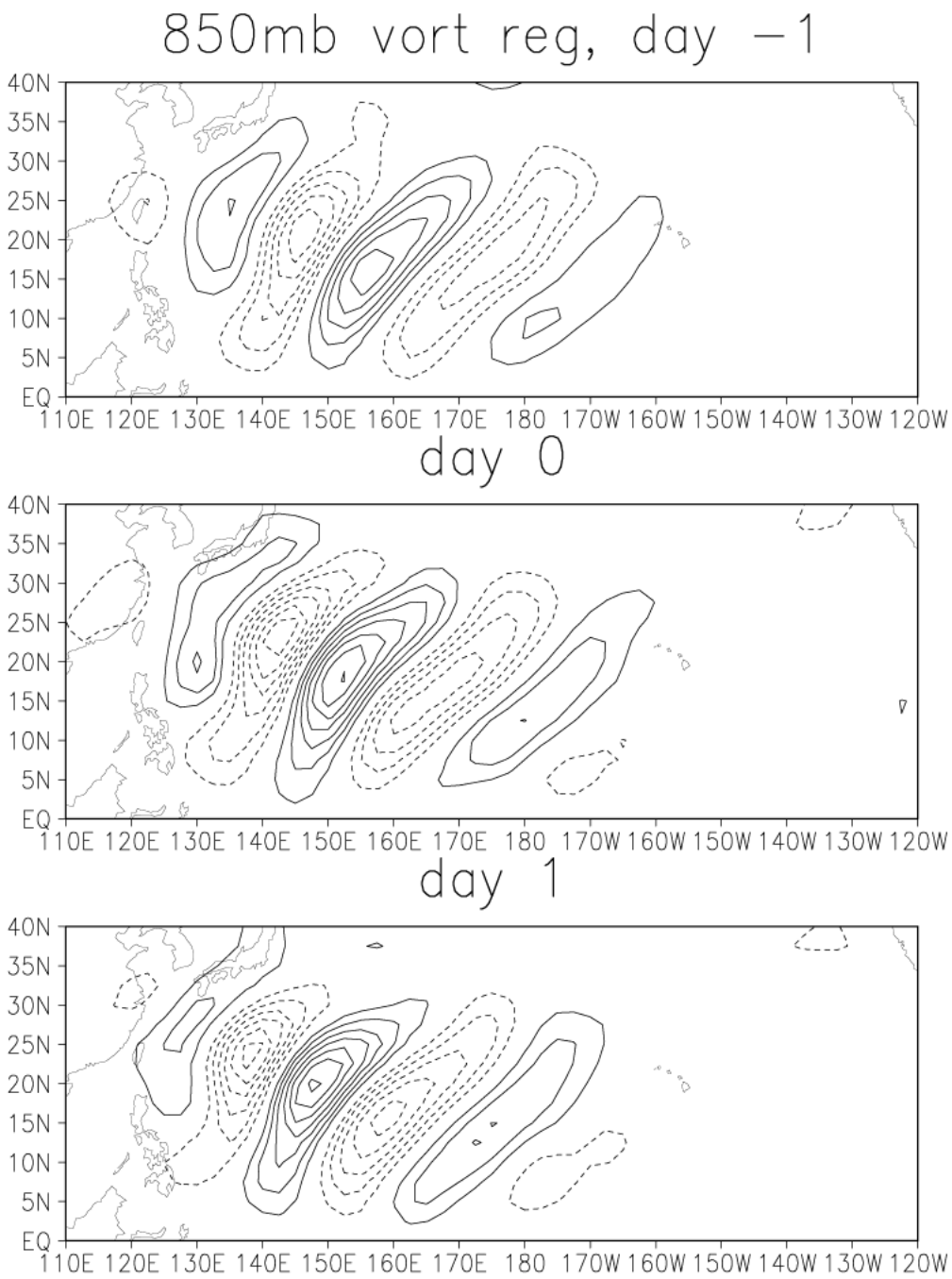

(from Tam and Li 2006)

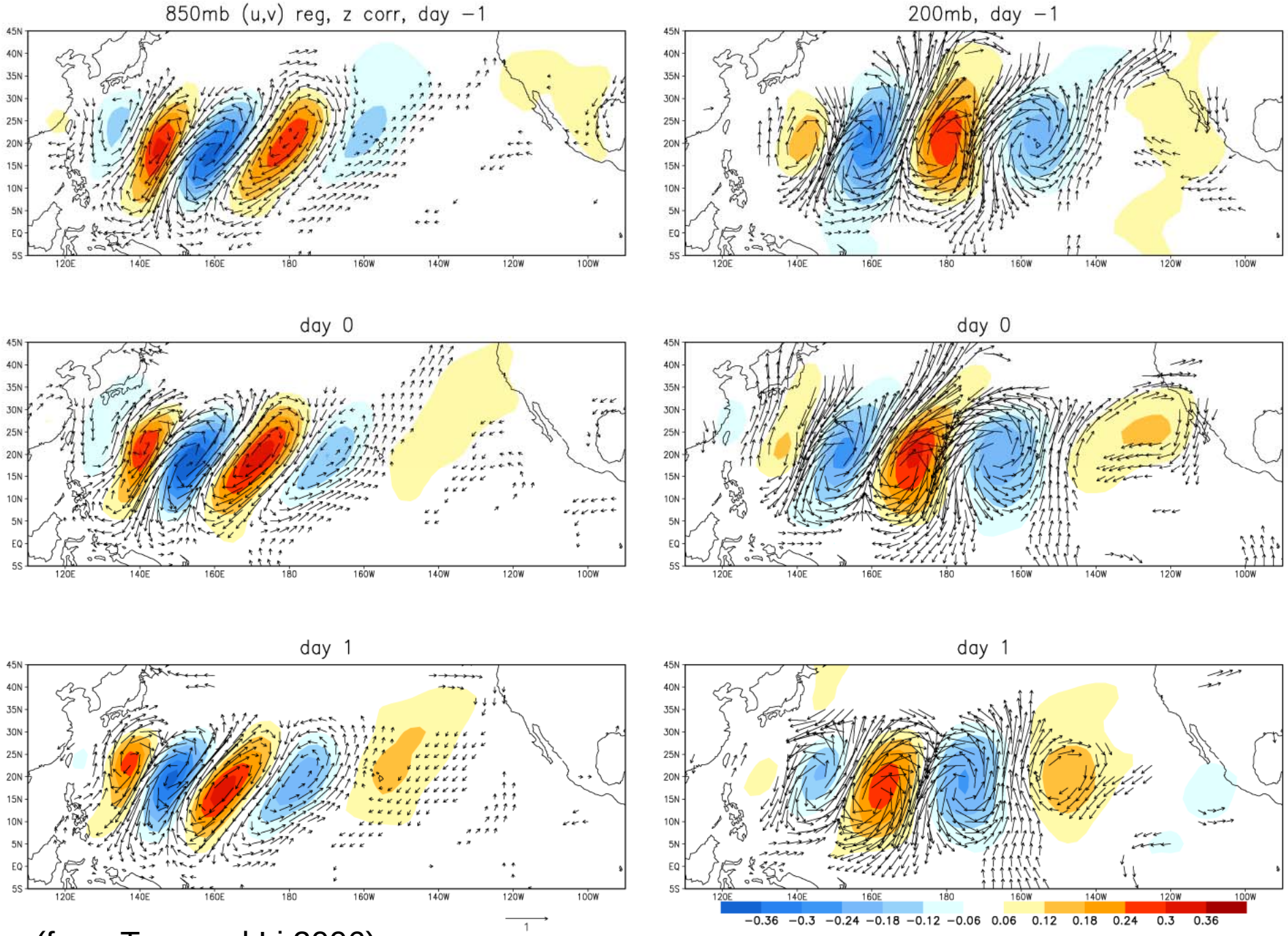

(from Tam and Li 2006)

Phase independent wave-activity flux (Takaya and Nakamura 01)

$$\mathbf{W} = \frac{\gamma}{2|\mathbf{U}|}\begin{pmatrix} U(\psi_x^{\,2} - \psi\psi_{xx}) + V(\psi_x\psi_y - \psi\psi_{xy}) \\ U(\psi_x\psi_y - \psi\psi_{xy}) + V(\psi_y^{\,2} - \psi\psi_{yy}) \\ \frac{f_0^{\,2}}{S_p}\left[U(\psi_x\psi_p - \psi\psi_{xp}) + V(\psi_y\psi_p - \psi\psi_{yp})\right] \end{pmatrix} + C_p\hat{\mathbf{U}}M$$

$$M = \frac{1}{2}\left(\frac{1}{2}\frac{q^2}{|\nabla Q|} + \frac{\gamma e}{|\mathbf{U}| - C_p}\right)$$

(γ = -1 for U < 0)

$$\partial_t M = -\nabla\cdot\mathbf{W} + S$$

In the plane wave limit, $\mathbf{W} = \mathbf{c}_g M$,

such that $-\nabla\cdot\mathbf{W} = -\mathbf{c}_g\cdot\nabla M - M\nabla\cdot\mathbf{c}_g$

(see Tam and Li 2006)

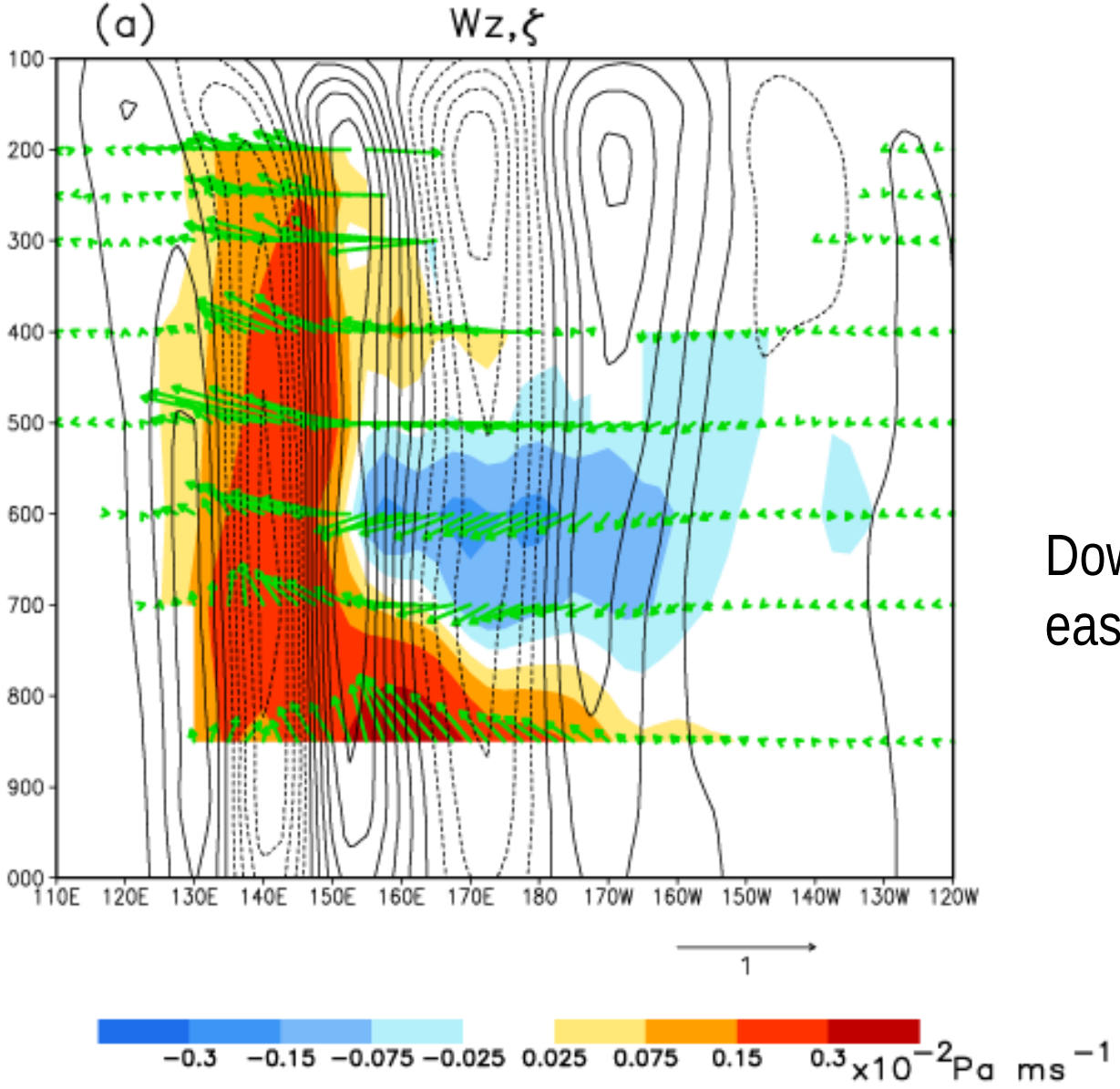

Downward activity flux east of 150°E

(from Tam and Li 2006)

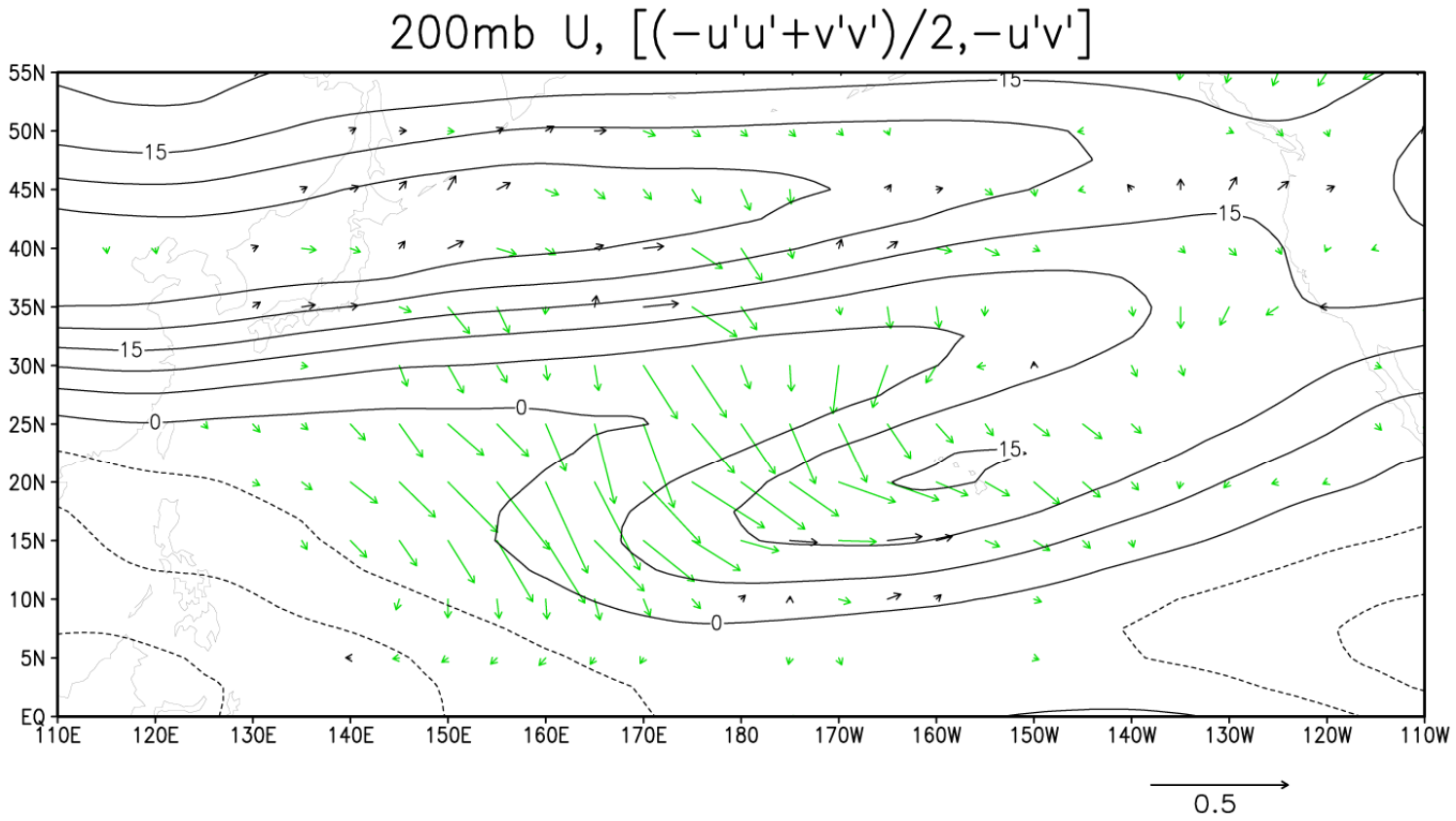

(green: −ve Ey; sum over day −4 to +4)

- Based on u' and v' related to the synoptic-scale waves
- Southward E vectors indicative of influence from mid latitudes

(from Tam and Li 2006)

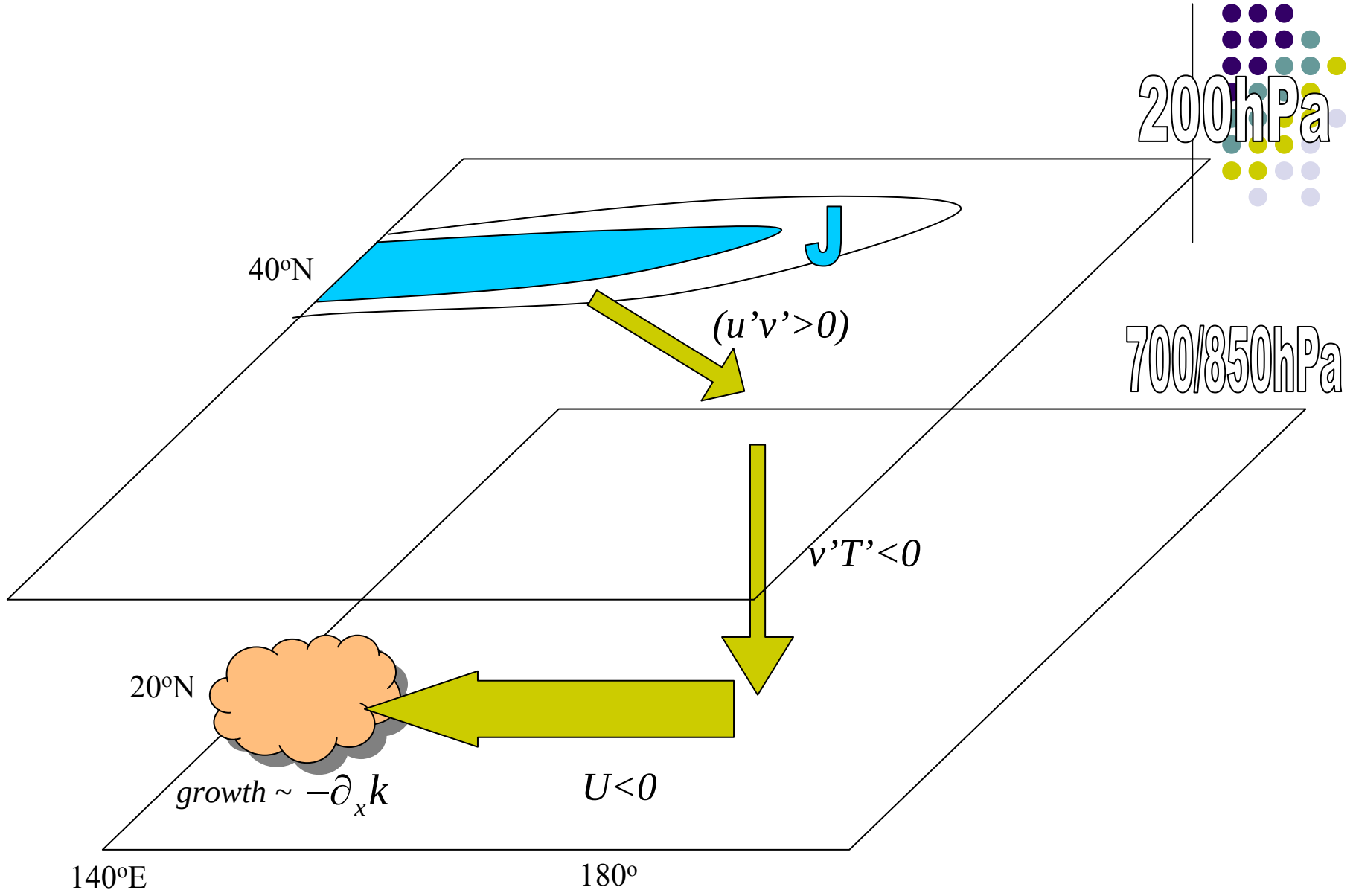

(based on Tam and Li 2006)

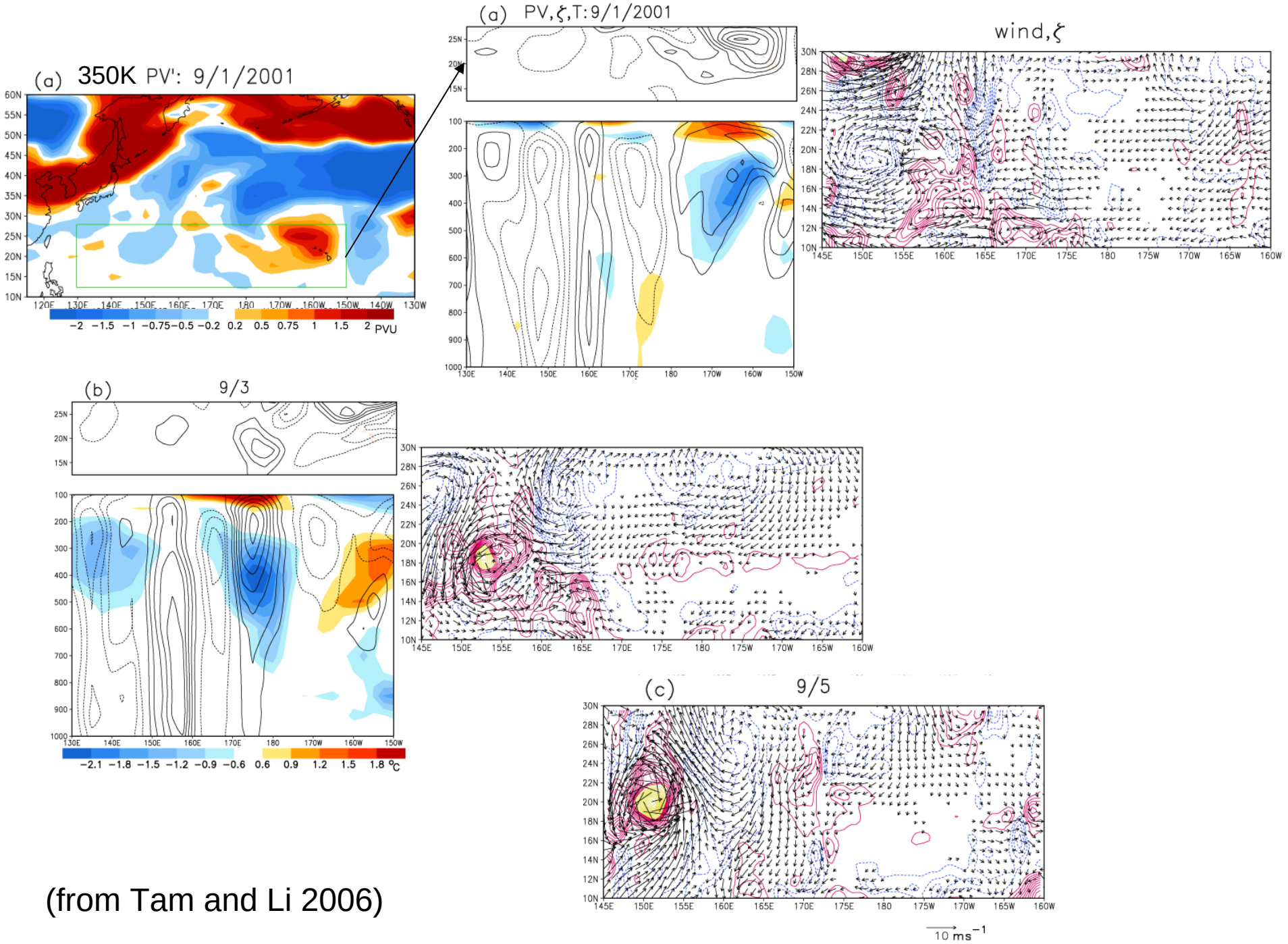

(from Tam and Li 2006)

References

- C.-P. Chang, Bin Wang and N.-C. G. Lau eds. *The Global Monsoon System: Research and Forecast*, **WMO/TD No. 1266,** 403-439.(available on Samba server: global_monsoon_system_IMW3.pdf)
- Madden, R.A., and P.R. Julian, 1994: Observations of the 40-50-day tropical oscillation- a review. *Mon. Wea. Rev.,* **122,** 814-837.
- Kemball-Cook, S., and B. Wang, 2001: Equatorial waves and air–sea interaction in the boreal summer intraseasonal oscillation. *J. Climate,* **14,** 2923-2942.
- Lau, K.-H., and N.-C. Lau, 1990: Observed structure and propagation characteristics of tropical summertime synoptic scale disturbances. *Mon. Wea. Rev.,* **118,** 1888-1913.
- Takaya, K., and H. Nakamura, 2001: A formulation of a phase-independent wave-activity flux for stationary and migratory quasigeostrophic eddies on a zonally varying basic flow. *J. Atmos. Sci.,* **58,** 608-627.
- Tam, C.-Y., and T. Li, 2006: The origin and dispersion characteristics of the observed tropical summertime synoptic-scale waves over the western Pacific. *Mon. Wea. Rev.,***134,** *1630-1646.*